Simulation of energetic particle driven geodesic acoustic modes and the energy channeling in the Large Helical Device plasmas

Simulation of energetic particle driven geodesic acoustic modes and the energy channeling in the Large Helical Device plasmas

Hao WANG (王 灝), Yasushi TODO (藤堂 泰), Masaki OSAKABE (長壁 正樹), Takeshi IDO (井戸 毅), Yasuhiro SUZUKI (鈴木 康浩)

National Institute for Fusion Science, National Institutes of Natural Sciences, Toki, Japan

E-mail: wanghao@nifs.ac.jp

November 2018

Abstract. Energetic particle driven geodesic acoustic modes (EGAMs) in the Large Helical Device (LHD) plasmas are investigated using MEGA code. MEGA is a hybrid simulation code for energetic particles interacting with a magnetohydrodynamic (MHD) fluid and in the present work, both the energetic particles and bulk ions are described by the kinetic equations. The low frequency EGAMs are reproduced. Also, the energy transfer is analyzed and the bulk ion heating during the EGAM activity is observed. The ions obtain energy when the energetic particles lose energy, and this indicates that an energy channel is established by EGAM. The EGAM channeling is reproduced by simulation with realistic parameters for the first time. The heating power to bulk ions is 3.4 kW/m^3. It is found that the sideband resonance is dominant during the energy transfer from EGAM to the bulk ions, and the transit frequencies of resonant bulk ions are one-half of the EGAM frequency.

1. Introduction

Geodesic acoustic mode (GAM) is an oscillatory zonal flow coupled with density and pressure perturbations in toroidal plasmas[1–6]. In the past decade, energetic particle driven GAM (EGAM) has been observed in JET, DIII-D, Large Helical Device (LHD), HL-2A, and ASDEX-Upgrade[7–13]. Many publications have been devoted to various aspects of EGAMs including the fundamental properties[14–31], the continuum damping[15, 32–34], the high frequency and low frequency branches[15, 35–38], and the half-frequency subcritical instabilities[39–41]. In the DIII-D experiment, the drops in neutron emission during the EGAM activities suggest beam ion losses[9]. Also, in the LHD experiment, anomalous bulk ion heating during the EGAM activity suggests an energy channel established by EGAM[42]. In addition, EGAMs interact with turbulence and thus affect the plasma transport and confinement[43, 44]. Then, the understanding

of the EGAMs is important for magnetic confinement fusion, because the energetic particles need to be well confined and the bulk plasma heating efficiency needs to be improved.

The EGAM channeling phenomenon has attracted the interest of many researchers because of the direct significance for plasma heating efficiency. The energy channel of GAM was discussed within the framework of quasilinear theory and the possibility of the GAM channeling was proved for the first time[45], and then, the energy transfer between particles and mode were simulated with a flat equilibrium profile for the first time[46]. In LHD, after observing the EGAM channeling for the first time[42], another investigation is being conducted to find the relation between EGAM channeling and the shear of safety factor[47]. However, at present, the existence of an EGAM energy channel has not been demonstrated by simulation with realistic parameters. In addition, although it is widely believed that the bulk ions obtain energy from EGAM via Landau damping, it is still not clear which resonant bulk ions are the dominant. The present paper is devoted to solving the above problems and demonstrating clear evidence, and it is organized as follows. In section 2, the simulation model and realistic parameters are described. In section 3, the linear properties of the simulated EGAM are shown, the EGAM channeling phenomenon in LHD is reproduced, and the mechanism of EGAM channeling is revealed. In section 4, the main conclusions are summarized.

2. Simulation model and parameters

A hybrid simulation code for energetic particles interacting with a magnetohydrodynamic (MHD) fluid, MEGA[48–52], is used for the simulations of EGAMs. We have two versions of MEGA. In the conventional version, only the energetic particles are described by the kinetic equations, while in the extended version not only the energetic particles but also the thermal ions are described kinetically. The simulation of the EGAM channeling is conducted with the extended version, and the simulation model is the same as Ref. [51]. This extended version is very important for EGAM channeling simulation, because the Landau damping process is a kind of wave-particle interaction process, and this process can be simulated only by the kinetic thermal ions model. In the past EGAM simulations by MEGA, the EGAM channeling was not found because of the MHD description of thermal ions. The following equations in the extended model are different from those in the conventional model:

$$\rho\frac{\partial}{\partial t}\mathbf{u}_{\mathbf{E}\perp} = -(\mathbf{M}\cdot\nabla)\mathbf{u}_{\mathbf{E}\perp} - \nabla p_e + (\mathbf{j} - \frac{Z_i e}{m_i}\rho_i\mathbf{v}_{\mathbf{pi}} - \frac{Z_h e}{m_h}\rho_h\mathbf{v}_{\mathbf{ph}})\times\mathbf{B}, \quad (1)$$

$$\mathbf{E} = -\mathbf{u}_{\mathbf{E}}\perp\times\mathbf{B} + \frac{\nabla_\parallel p_e}{(-e)n_e} + \eta(\mathbf{j} - \mathbf{j}_{\mathbf{eq}}), \quad (2)$$

$$\rho = \rho_i + \rho_h, \quad (3)$$

$$\mathbf{M} = \rho\mathbf{u}_{\mathbf{E}\perp} + (\rho_i v_{i\parallel} + \rho_h v_{h\parallel})\mathbf{b} + \rho_i\mathbf{v}_{\mathbf{pi}} + \rho_h\mathbf{v}_{\mathbf{ph}}, \quad (4)$$

$$\rho_i \mathbf{v_{pi}} = \frac{m_i}{Z_i e}(-\frac{\nabla p_{i\perp} \times \mathbf{B}}{B^2} + (p_{i\parallel} - p_{i\perp})\frac{\nabla \times \mathbf{b}}{B}). \quad (5)$$

The subscript h denotes the hot particles or the energetic particles, and the subscript i denotes the bulk ions. The Eq.(1) is momentum equation, and Eq.(2) is Ohm's law. The particle-in-cell (PIC) method is applied for ρ_i, ρ_h, $\rho_i v_{i\parallel}$, $\rho_h v_{h\parallel}$, $p_{i\parallel}$, $p_{i\perp}$, $p_{h\parallel}$, and $p_{h\perp}$. The switch of collision is turned off in the present simulation, thus the bulk ions cannot absorb any energy from energetic particles via collision processes. This turning off operation is reasonable because the beam velocity is higher than critical velocity[53], and the similar operation can be found in Ref. [18].

A realistic 3-dimensional equilibrium generated by HINT code is used for the simulation[54]. This equilibrium data is based on the LHD shot #109031 at time $t = 4.94$ s. At this moment, the EGAM activity is very strong, thus it is good for reproducing the EGAM phenomenon. In LHD, the EGAM frequency should be similar to that in tokamaks[3, 4]. The energy of neutral beam injection (NBI) is high, thus it is possible to excite a high frequency branch of EGAM under the condition of bump-on-tail distribution[36, 37], while the high frequency branch has not been observed in tokamaks. The following six parameters for the EGAM simulation are based on an LHD experiment[42]: 1) The plasma major radius $R_0 = 3.75$ m. 2) The magnetic field strength on the magnetic axis $B_0 = 1.5$ T. 3) The electron density in plasma center $n_e = 0.072 \times 10^{19}$ m^{-3}, and density profile is the same as experiment. 4) The safety factor $q = 2.82$ on the magnetic axis, and $q = 0.83$ on the plasma edge. 5) The injected neutral beam energy is $E_{NBI} = 170$ keV. And finally, 6) a Gaussian-type pitch angle distribution function is assumed for the energetic particles, and the distribution function peaks at $\Lambda = 0.1$ where $\Lambda = \mu B_0/E$ is the pitch angle variable, μ is the magnetic moment, and E is the particle energy. A slowing-down energetic particle distribution function and a Maxwellian bulk ion distribution are assumed in the paper.

The number of computational particles is 8 million for both energetic particles and bulk ions, but a larger number of particles, 67 million, is also used to decrease the noise and to investigate the numerical convergence. Cylindrical coordinates (R, ϕ, z) are employed. For LHD equilibrium, there are ten pitches in the toroidal direction (ϕ direction). Since the toroidal mode number of the GAM is $n = 0$, for simplicity, only one pitch from $\phi = 0$ to $\phi = 0.2\pi$ is used for the present simulation, while the other nine pitches from $\phi = 0.2\pi$ to $\phi = 2\pi$ are obtained by periodic extension. This simplification is made to save computational resources and time. The numbers of grid points of this pitch in the (R, ϕ, z) directions are (128, 64, 128), respectively. The viscosity and diffusivity are set to be $\nu = \nu_n = 4.5 \times 10^{-7} v_A R_0 = 64.97$ m^2/s and the resistivity $\eta = 4.5 \times 10^{-7} \mu_0 v_A R_0 = 8.16 \times 10^{-5}\ \Omega \cdot$ m in the simulation, where v_A is the Alfvén velocity at the plasma center.

3. Simulation results

3.1. Mode linear properties

The spatial profile of the simulated mode is shown in Fig. 1. This mode peaks around $r/a = 0.2$, very close to the plasma center. The mode width is as large as approximately $0.4a$, thus the simulated mode is identified as a global mode. Figure 2 shows the mode frequency and amplitude versus radial position to confirm the global property. The frequency profile is spatially constant. This is similar with Fig. 2(c) of Ref. [9] and Fig. 6 of Ref. [20]. The global mode structure is caused by large orbit width of energetic particles, and it is consistent with Fig. 4 of Ref. [14]. The dominant mode number is $m/n = 0/0$ for poloidal velocity v_θ as represented by the red curve in Fig. 1(a). The components weaker than 4.31×10^{-5} (10% of the peak value of the 0/0 cosine component) are considered as negligible and thus they are not plotted. Also, the dominant mode number is $m/n = 1/0$ for pressure perturbation δP as shown in Fig. 1(b). Similarly, the components weaker than 10% of the peak value of the 1/0 sine component are not plotted. These mode numbers are consistent with the nature of GAM and EGAM[1, 2, 14, 20]. The dominant component of poloidal velocity v_θ is the cosine part because sine part is zero for $m/n = 0/0$. The dominant component of pressure perturbation δP is the sine part because the density accumulation is proportional to $\tilde{\mathbf{E}} \times \mathbf{B} \cdot \nabla B^2/B^4$ where $\tilde{\mathbf{E}}$ is the fluctuating electric field[1]. Finally, the magnetic perturbation exists, but it is much weaker than the poloidal velocity perturbation, and this indicates that the mode is an electrostatic mode. This is also consistent with the nature of EGAM[14]. Thus, according to the above three features of mode width, mode number, and weak magnetic perturbation, the simulated global electrostatic mode is identified as an EGAM. This is the first time to reproduce an EGAM using the extended model of MEGA code.

In addition, the simulated EGAMs' linear frequencies are between 40 kHz to 50 kHz as shown in Fig. 3, and are lower than the theoretically predicted conventional GAM frequency 54 kHz. Thus, these are low frequency branches of EGAM. The mode frequency decreases with increasing β_{EP}, which is the ratio of the energetic particle pressure to the magnetic pressure, and this frequency decreasing is consistent with the EGAM property[9, 14, 18, 20, 46]. The mode frequencies are lower than GAM frequency because the energetic particles contribute negatively to the mode frequency under the condition of slowing-down energetic particle distribution function.

3.2. The reproduced phenomenon of EGAM channeling

A typical case where $\beta_{EP} = 0.04\%$ is used to demonstrate the EGAM channeling phenomenon is shown in Fig. 4. Figure 4(a) shows the frequency spectrum of simulated EGAM. The mode frequency in linear stage is 50 kHz, and then, the frequency chirps up in the nonlinear stage. At $t = 0.5$ ms, the frequency has already exceeded 60 kHz. The frequency chirping rate $d\omega/dt$ gradually decreases with time. Fig. 4(b) shows the time

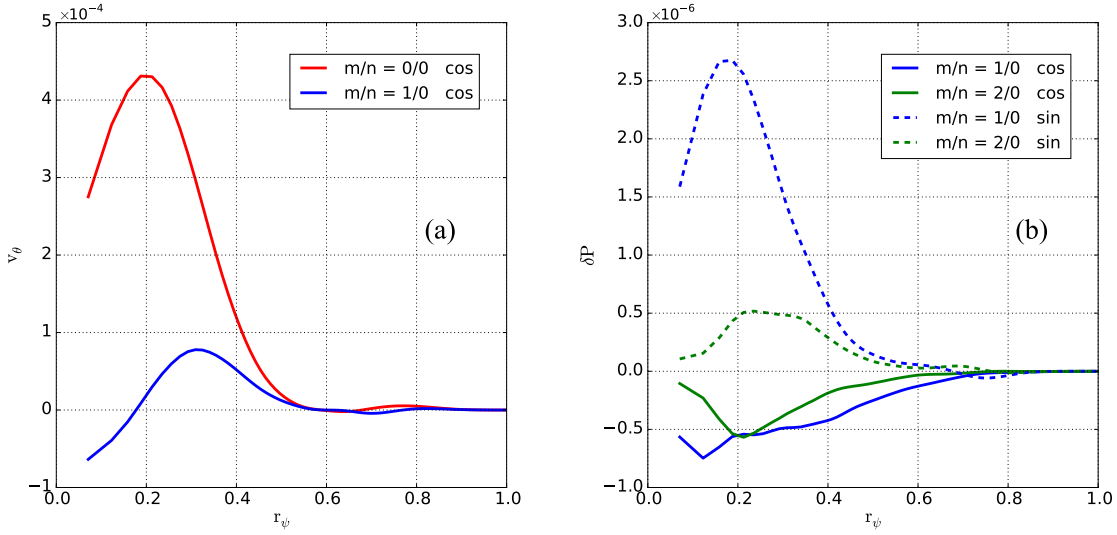

Figure 1. The simulated mode profile of (a) poloidal velocity v_θ with dominant mode number $m/n = 0/0$ and (b) pressure perturbation δP with dominant mode number $m/n = 1/0$.

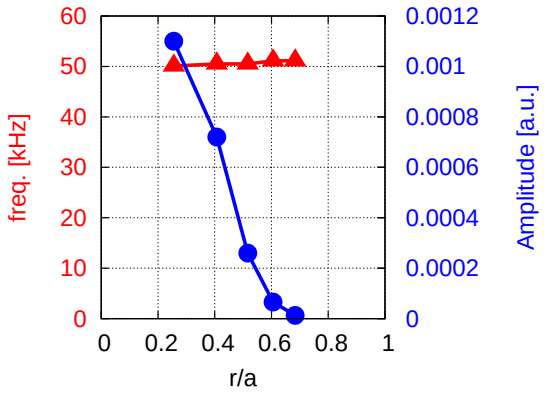

Figure 2. The mode frequency and amplitude versus radial position.

evolution of EGAM amplitude v_θ. The linear stage is from $t = 0$ to about $t = 0.1$ ms. At $t = 0.1$ ms, the mode amplitude reaches the maximum value, and then steps into the nonlinear stage. Fig. 4(c) shows the energy transfer of various species. The energy transfer to each species is analyzed by the volume integration and time integration $E_{trans} = \int_0^t dt' \int \mathbf{j} \cdot \mathbf{E} dV$. Here, $\mathbf{j}$ stands for the perpendicular current of the species, which consists of ∇B drift current, curvature drift current, and magnetization current. $\mathbf{E}$ is the ideal MHD electric field $-\mathbf{v} \times \mathbf{B}$. For energetic particles and bulk ions, ∇B drift current and magnetization current are given by perpendicular pressure, and curvature drift current is given by parallel pressure. For electron, the perpendicular and parallel pressures are replaced by a scalar pressure. This is equivalent to the diamagnetic current $\mathbf{j} = \frac{-\nabla p \times \mathbf{B}}{B^2}$. The bulk ion heating during the EGAM activity is observed. The ions

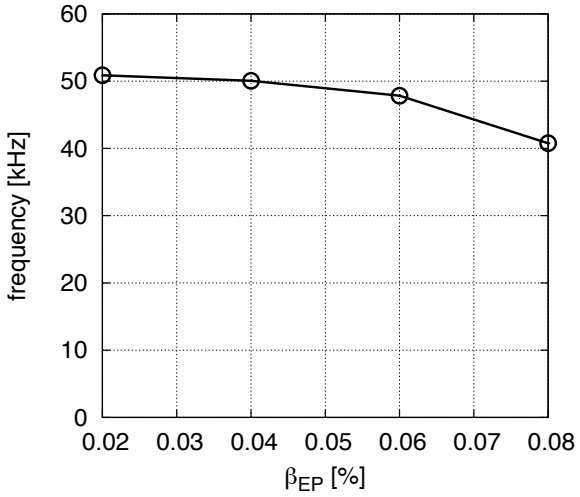

Figure 3. The energetic particle pressure dependence of EGAM frequency in the linear growth phase.

obtain energy when the energetic particles lose energy, and this indicates that an energy channel is established by EGAM. The EGAM channeling is reproduced by simulation with realistic parameters for the first time. The first demonstration of energy exchange between EGAM and thermal plasma was made in 2014[46], but a flat equilibrium profile was applied. In the present work, from $t = 0$ to $t = 0.36$ ms, the energy transferred from energetic particles is 63 J. About one-half of this energy (51%) is transferred to bulk ions (34%) and electrons (17%), while the other half is dissipated by the terms of ν, ν_n, and η. The heating power to bulk ions around $t = 0.1$ ms is 3.4 kW/m^3.

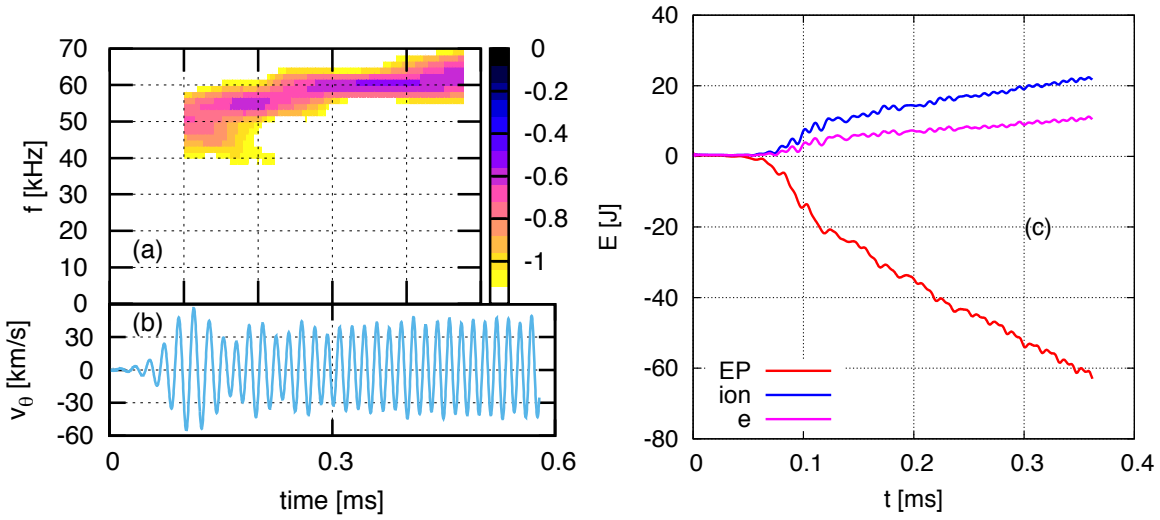

Figure 4. (a) The frequency spectrum of EGAM. (b) The time evolution of EGAM amplitude v_θ. (c) Energy transfer of various species during EGAM activity. EP is the abbreviation of energetic particle.

3.3. The mechanism of EGAM channeling

In order to identify the dominant resonant particles, the δf distribution of both energetic particles and bulk ions at different times are analyzed in the particle transit frequency space, as shown in Fig. 5. The particle transit frequency f_{tr} is defined by $f_{tr} = v_{\parallel}/(2\pi q R_0)$, where $v_{\parallel}$ is particle parallel velocity. For simplicity of f_{tr} calculation, $q = 2.8$ is a constant for all the particles in the above f_{tr} equation, although q value has a normal shear profile in the equilibrium of simulation. The simplicity of constant q is reasonable because most resonant particles are located around the $q = 2.8$ region. The EGAM obtains energy from energetic particles via inverse Landau damping, and EGAM transfer energy to bulk ions via Landau damping. These processes modify the distribution function of both energetic particles and bulk ions, and thus, δf values change with mode evolution. The particles with negative δf values form the hole structure in phase space, and the particles with positive δf values form the clump structure. Large absolute δf values indicate strong interactions between EGAM and resonant particles. Fig. 5(a) shows the δf of energetic particles. A hole around $f_{tr} = 50$ kHz is formed. The bottom of this hole moves rightward. This indicates that the transit frequencies of particles in the hole increase with time and this increase of frequency is kept consistent with the chirping up of EGAM frequency. The resonance condition between EGAM and energetic particles is given by $f_{EGAM} = f_{tr,EP}$. Fig. 5(b) shows the δf of bulk ions. Two clumps around $f_{tr} = 25$ kHz and $f_{tr} = 5$ kHz are formed. The peaks of these clumps move rightward. This indicates that the transit frequencies of bulk ions in these clumps increase with time and these transit frequencies are kept at the half of the EGAM frequency (and one-tenth of the EGAM frequency). The resonance condition between EGAM and bulk ions is given by

$$f_{EGAM} = l \cdot f_{tr,bulk}, \tag{6}$$

and dominant l values are $l = 2$ and $l = 10$. The resonant condition $l = 2$ is similar to Fig. 4 and Fig. 5 in Ref. [55]. Sideband resonance is important for the interaction between EGAM and bulk ions. This is the first time to quantitatively reveal the resonance condition between EGAM and bulk ions during the establishment of EGAM channeling.

The resonant particles in μ phase space and in radial spatial space are also analyzed. It is found that the μ values of dominant resonant energetic particles are relatively higher, while the μ values of dominant resonant bulk ions are relatively lower. This indicates that the high-μ energetic particles excite the mode and the low-μ bulk ions absorb energy. This is similar with that in Ref. [18]. For the spatial distribution, it is found that 99% resonant energetic particles distribute around the core region where r/a<0.7.

In Eq. (6), $l = 2$ is important because $l = 2$ sideband resonance condition is much easier to be satisfied than higher l value cases. However, $l = 10$ corresponds to the resonant ions with very low transit frequencies, and these low transit frequency ions can hardly obtain energy from EGAM. In order to confirm that, the energy transfer rate

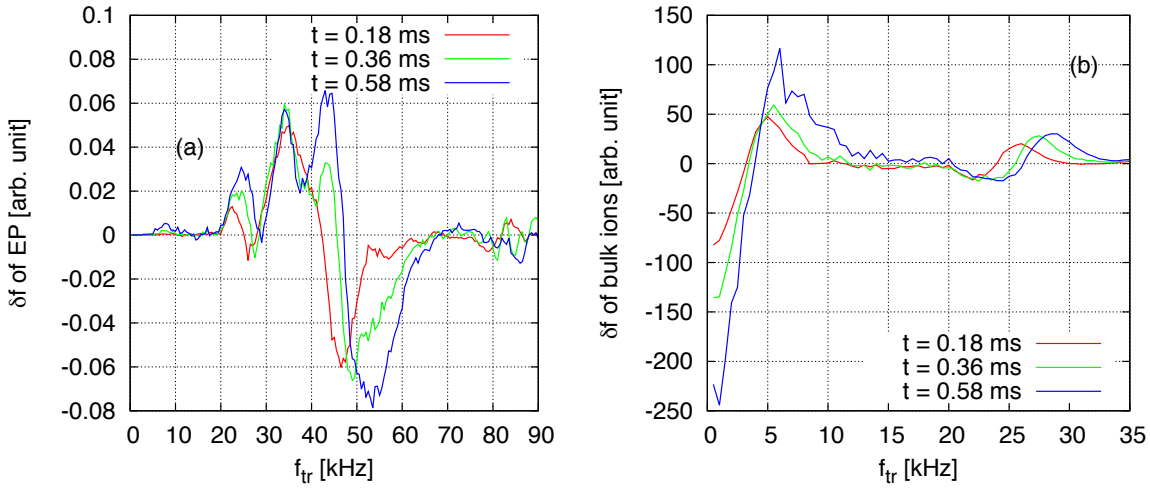

Figure 5. The δf distributions of (a) energetic particles and (b) bulk ions in f_{tr} phase space at $t = 0.18$ ms (red), $t = 0.36$ ms (green), and $t = 0.58$ ms (blue). EP is the abbreviation of energetic particle.

$dE/dt \cdot \delta f$ of bulk ions in f_{tr} phase space is analyzed as shown in Fig. 6. There is a peak around $f_{tr} = 25$ kHz, and this peak gradually moves rightward. Similar to Fig. 5(b), this rightward movement indicates that the bulk ions with the half of the mode frequency are kept resonant with the mode. The energy transfer rate is positive, and this indicates that the bulk ions absorb energy from EGAM. In Fig. 6, the red curve at $t = 0.109$ ms represents the time of transition between linear growth stage and nonlinear frequency chirping stage. At this time, the peak value of $dE/dt \cdot \delta f$ is very large because the mode amplitude is very large as shown in Fig. 4(b) and the energy transfer rate is also large as shown in Fig. 4(c). Then gradually, the peak values around $f_{tr} = 25$ kHz decrease with time, because the energy transfer rates decrease, which is also consistent with Fig. 4(c). It is very significant that the high frequency (high energy) bulk ions absorb energy from EGAM. Since the bulk ion temperature is high in ITER-like device, it is possible to infer that the EGAM channeling may improve the heating efficiency in ITER, although the present paper is based on a stellarator configuration. From $t = 0.145$ ms in the fully nonlinear stage, a lower peak appears around $f_{tr} = 15$ kHz. In this simulation, the bulk ion temperature $T_i = 4.85$ keV, and this thermal velocity corresponds to a transit frequency 14.7 kHz. The lower peak around $f_{tr} = 15$ kHz appears in Fig. 6 because most bulk ions' transit frequencies are around 15 kHz. In Fig. 5(b), there is a peak around 5 kHz, but this peak is very weak and difficult to identify in Fig. 6, because the particles around 5 kHz do not absorb too much energy. The bulk ions mainly absorb energy via the particles whose transit frequencies are the half of the EGAM frequency. In Eq. 6, $l = 2$ is more important than $l = 10$ for the establishment of EGAM channeling.

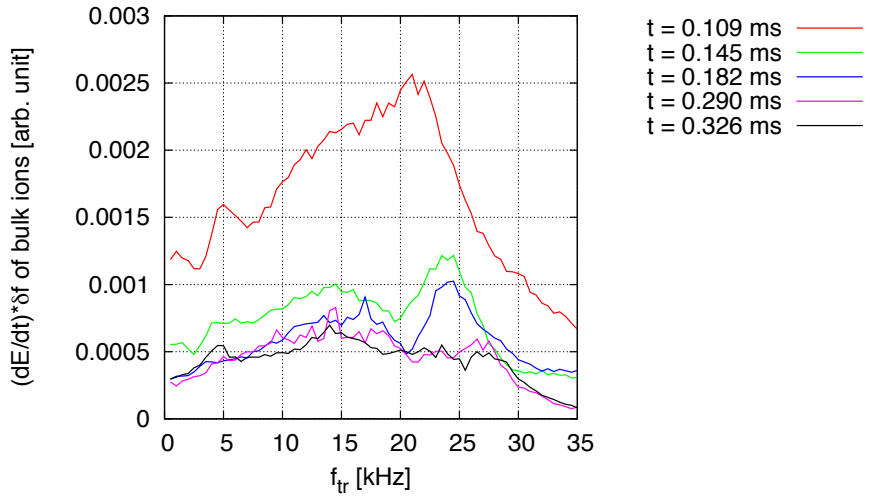

Figure 6. Energy transfer rate $dE/dt \cdot \delta f$ of bulk ions in transit frequency f_{tr} phase space at different times.

3.4. Numerical convergence

In order to confirm that the simulation results are reliable and the number of simulation particles is sufficient, numerical convergence has been investigated with regard to the number of particles. Four cases with different numbers of particles are compared at $r/a = 0.26$. The smallest particle number case was run with $2^{23} = 8.39 \times 10^6$ energetic particles and the same number of bulk ions, while the largest particle number case was run with $2^{26} = 6.71 \times 10^7$ energetic particles and the same number of bulk ions. In other two case, the particle numbers are in between. The time evolutions of poloidal velocity v_θ are shown in Fig. 7. For the smallest particle number case, the mode linear growth rate and the frequency are 12.4% and 50.1 kHz, respectively. For the largest particle number case, the growth rate is 13.7% and the frequency is 50.7 kHz. The difference of linear growth rates is about 10%, and the difference of mode frequencies is only 1.2%. According to this comparison, it can be concluded that the numerical convergence is good enough for the results presented in this paper.

4. Summary

In summary, a global electrostatic mode is reproduced using the extended version of MEGA code, and the simulated mode is identified as an EGAM. Both the mode number and the mode frequency are consistent with the theoretical predictions. The ions obtain energy when the energetic particles lose energy during the EGAM activity, and this indicates that an energy channel is established by EGAM. The EGAM channeling is reproduced by simulation with realistic parameters for the first time. The heating power to bulk ions is 3.4 kW/m^3. The δf distribution of both energetic particles and bulk ions at different times are investigated, and the transit frequencies of resonant particles are

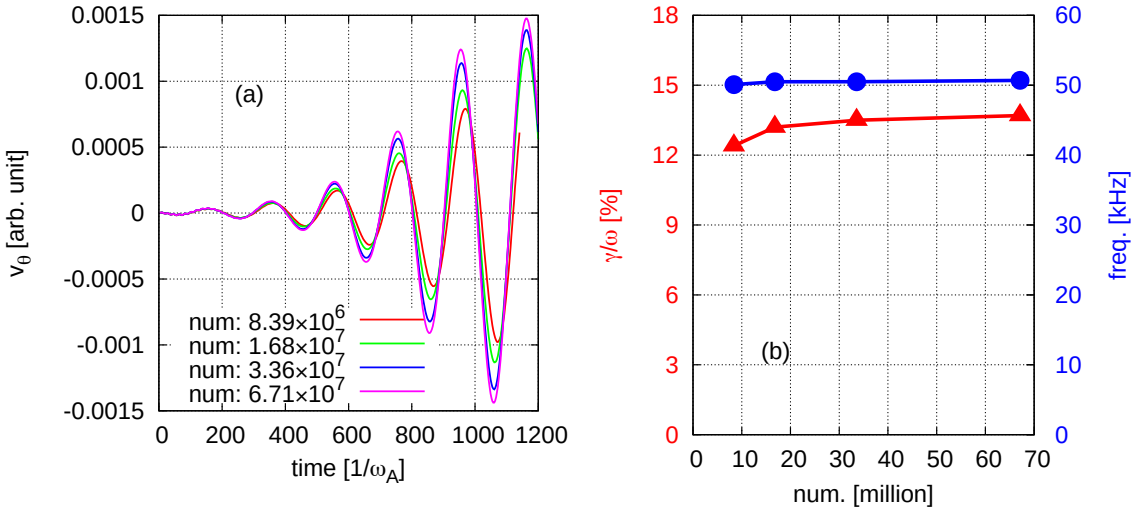

Figure 7. (a) Time evolution of poloidal velocity v_θ for different numbers of particles. Four cases with different numbers of energetic particles are compared, and the number of bulk ions is identical with that of energetic particles. (b) Linear growth rates and frequencies versus the numbers of energetic particles.

analyzed. Also, the energy transfer rate of bulk ions at different times are investigated and compared with δf distribution. The resonance condition $f_{EGAM} = l \cdot f_{tr,bulk}$ is satisfied where the dominant l values is $l = 2$. Another resonance with $l = 10$ was also found. The resonance condition between EGAM and bulk ions during the establishment of EGAM channeling is quantitatively revealed in the present work.

Acknowledgments

Numerical computations were performed on the "Plasma Simulator" (FUJITSU FX100) of National Institute for Fusion Science (NIFS) with the support and under the auspices of the NIFS Collaboration Research program (NIFS17KNST111, NIFS18KNST136, and NIFS18KNXN365), and the "K Computer" of the RIKEN Advanced Institute for Computational Science (Project ID: hp170260 and hp180200). This work was partly supported by MEXT as "Priority Issue on Post-K Computer" (Accelerated Development of Innovative Clean Energy Systems), JSPS KAKENHI Grant No. JP18K13529, and JSPS KAKENHI Grant No. JP18H01202. The authors thank Prof. H. Sugama, Prof. K. Toi, Dr. K. Shinohara, and Prof. D. Zarzoso for fruitful discussions.

References

[1] Winsor N, Johnson J and Dawson J 1968 *Physics of Fluids* **11** 2448 ISSN 0031-9171 URL `http://dx.doi.org/10.1063/1.1691835`

[2] Diamond P H, Itoh S I, Itoh K and Hahm T S 2005 *Plasma*

Physics and Controlled Fusion **47** R35–R161 ISSN 1361-6587 URL http://dx.doi.org/10.1088/0741-3335/47/5/R01

[3] Watari T, Hamada Y, Notake T, Takeuchi N and Itoh K 2006 *Physics of Plasmas* **13** 062504 (*Preprint* https://doi.org/10.1063/1.2206170) URL https://doi.org/10.1063/1.2206170

[4] Sugama H and Watanabe T H 2006 *Physics of Plasmas* **13** 012501 ISSN 1089-7674 URL http://dx.doi.org/10.1063/1.2149311

[5] Zonca F and Chen L 2008 *EPL (Europhysics Letters)* **83** 35001 URL https://doi.org/10.1209%2F0295-5075%2F83%2F35001

[6] Chen L, Qiu Z and ZoncaF 2014 *Europhysics Letters* **107** 15003 (*Preprint* https://doi.org/10.1209/0295-5075/107/15003) URL https://doi.org/10.1209/0295-5075/107/15003

[7] Berk H, Boswell C, Borba D, Figueiredo A, Johnson T, Nave M, Pinches S, Sharapov S and contributors J E 2006 *Nuclear Fusion* **46** S888–S897 URL https://doi.org/10.1088%2F0029-5515%2F46%2F10%2Fs04

[8] Boswell C, Berk H, Borba D, Johnson T, Pinches S and Sharapov S 2006 *Physics Letters A* **358** 154 – 158

[9] Nazikian R, Fu G Y, Austin M E, Berk H L, Budny R V, Gorelenkov N N, Heidbrink W W, Holcomb C T, Kramer G J, McKee G R, Makowski M A, Solomon W M, Shafer M, Strait E J and Zeeland M A V 2008 *Phys. Rev. Lett.* **101**(18) 185001 URL https://link.aps.org/doi/10.1103/PhysRevLett.101.185001

[10] Ido T, Shimizu A, Nishiura M, Nakamura S, Kato S, Nakano H, Yoshimura Y, Toi K, Ida K, Yoshinuma M, Satake S, Watanabe F, Morita S, Goto M, Itoh K, Kubo S, Shimozuma T, Igami H, Takahashi H, Yamada I, Narihara K and the LHD Experiment Group 2011 *Nuclear Fusion* **51** 073046 URL http://stacks.iop.org/0029-5515/51/i=7/a=073046

[11] Chen W, Ding X, Yu L, Ji X, Shi Z, Zhang Y, Zhong W, Yuan G, Dong J, Yang Q, Liu Y, Yan L, Zhou Y, Jiang M, Li W, Song X, Chen S and and X D 2013 *Nuclear Fusion* **53** 113010 URL https://doi.org/10.1088%2F0029-5515%2F53%2F11%2F113010

[12] Horváth L, Papp G, Lauber P, Por G, Gude A, Igochine V, Geiger B, Maraschek M, Guimarais L, Nikolaeva V, Pokol G and the ASDEX Upgrade Team 2016 *Nuclear Fusion* **56** 112003 URL http://stacks.iop.org/0029-5515/56/i=11/a=112003

[13] Lauber P, Geiger B, Papp G, Por G, Pokol G I, Poloskei P Z, Guimarais L, Maraschek M, Igochine V, Hayward-Schneider T, Lu Z, Wang X, Conway G, the ASDEX Upgrade Team and the Eurofusion Enabling Research 'NAT' Team 2018 Strongly non-linear energetic particle dynamics in asdex upgrade scenarios with core impurity accumulation *27th IAEA Fusion Energy Conference Proceedings*

[14] Fu G Y 2008 *Phys. Rev. Lett.* **101**(18) 185002 URL https://link.aps.org/doi/10.1103/PhysRevLett.101.185002

[15] Qiu Z, Zonca F and Chen L 2010 *Plasma Physics and Controlled Fusion* **52** 095003 URL http://stacks.iop.org/0741-3335/52/i=9/a=095003

[16] Berk H and Zhou T 2010 *Nuclear Fusion* **50** 035007 URL http://stacks.iop.org/0029-5515/50/i=3/a=035007

[17] Qiu Z and Chen L 2011 *Plasma Science and Technology* **13** 257–266 URL https://doi.org/10.1088%2F1009-0630%2F13%2F3%2F01

[18] Zarzoso D, Garbet X, Sarazin Y, Dumont R and Grandgirard V 2012 *Physics of Plasmas* **19** 022102 (*Preprint* https://doi.org/10.1063/1.3680633) URL https://doi.org/10.1063/1.3680633

[19] Fisher R, Pace D, Kramer G, Zeeland M V, Nazikian R, Heidbrink W and García-Muñoz M 2012 *Nuclear Fusion* **52** 123015 URL https://doi.org/10.1088%2F0029-5515%2F52%2F12%2F123015

[20] Wang H and Todo Y 2013 *Physics of Plasmas* **20** 012506 ISSN 1089-7674 URL http://dx.doi.org/10.1063/1.4774410

[21] Wang H, Todo Y and Kim C C 2013 *Phys. Rev. Lett.* **110**(15) 155006 URL https://link.aps.org/doi/10.1103/PhysRevLett.110.155006

[22] Ren H and Cao J 2014 *Physics of Plasmas* **21** 122512 (*Preprint* https://doi.org/10.1063/1.4903911) URL https://doi.org/10.1063/1.4903911

[23] Girardo J B, Zarzoso D, Dumont R, Garbet X, Sarazin Y and Sharapov S 2014 *Physics of Plasmas* **21** 092507 (*Preprint* https://doi.org/10.1063/1.4895479) URL https://doi.org/10.1063/1.4895479

[24] Biancalani A, Bottino A, Lauber P and Zarzoso D 2014 *Nuclear Fusion* **54** 104004 URL https://doi.org/10.1088%2F0029-5515%2F54%2F10%2F104004

[25] Ren H 2016 *Nuclear Fusion* **57** 016023 URL https://doi.org/10.1088%2F0029-5515%2F57%2F1%2F016023

[26] Kolesnichenko Y I, Lutsenko V V, Yakovenko Y V, Lepiavko B S, Grierson B, Heidbrink W W and Nazikian R 2016 *Plasma Physics and Controlled Fusion* **58** 045024 URL https://doi.org/10.1088%2F0741-3335%2F58%2F4%2F045024

[27] Qu Z S, Hole M J and Fitzgerald M 2016 *Phys. Rev. Lett.* **116**(9) 095004 URL https://link.aps.org/doi/10.1103/PhysRevLett.116.095004

[28] Sasaki M, Kasuya N, Itoh K, Hallatschek K, Lesur M, Kosuga Y and Itoh S I 2016 *Physics of Plasmas* **23** 102501 (*Preprint* https://doi.org/10.1063/1.4963397) URL https://doi.org/10.1063/1.4963397

[29] Zarzoso D, Migliano P, Grandgirard V, Latu G and Passeron C 2017 *Nuclear Fusion* **57** 072011 URL https://doi.org/10.1088%2F1741-4326%2Faa7351

[30] Biancalani A, Chavdarovski I, Qiu Z, Bottino A, Sarto D D, Ghizzo A, Gurcan O, Morel P and Novikau I 2017 *Journal of Plasma Physics* **83** 725830602

[31] Qu Z S, Hole M J and Fitzgerald M 2017 *Plasma Physics and Controlled Fusion* **59** 055018 URL https://doi.org/10.1088%2F1361-6587%2Faa6636

[32] Qiu Z, Zonca F and Chen L 2012 *Physics of Plasmas* **19** 082507 (*Preprint* https://doi.org/10.1063/1.4745191) URL https://doi.org/10.1063/1.4745191

[33] Palermo F, Biancalani A, Angioni C, Zonca F and Bottino A 2016 *EPL (Europhysics Letters)* **115** 15001 URL https://doi.org/10.1209%2F0295-5075%2F115%2F15001

[34] Biancalani A, Palermo F, Angioni C, Bottino A and Zonca F 2016 *Physics of Plasmas* **23** 112115 (*Preprint* https://doi.org/10.1063/1.4967703) URL https://doi.org/10.1063/1.4967703

[35] Cao J, Qiu Z and Zonca F 2015 *Physics of Plasmas* **22** 124505 (*Preprint* https://doi.org/10.1063/1.4938277) URL https://doi.org/10.1063/1.4938277

[36] Wang H, Todo T, Ido T and Osakabe M 2015 *Physics of Plasmas* **22** 092507 ISSN 1089-7674 URL http://dx.doi.org/10.1063/1.4930130

[37] Ido T, Osakabe M, Shimizu A, Watari T, Nishiura M, Toi K, Ogawa K, Itoh K, Yamada I, Yasuhara R, Yoshimura Y, Kato S and Group T L E 2015 *Nuclear Fusion* **55** 083024 URL http://stacks.iop.org/0029-5515/55/i=8/a=083024

[38] Ren H and Wang H 2018 *Nuclear Fusion* **58** 046005 URL http://stacks.iop.org/0029-5515/58/i=4/a=046005

[39] Ido T, Itoh K, Osakabe M, Lesur M, Shimizu A, Ogawa K, Toi K, Nishiura M, Kato S, Sasaki M, Ida K, Inagaki S and Itoh S I (the LHD Experiment Group) 2016 *Phys. Rev. Lett.* **116**(1) 015002 URL https://link.aps.org/doi/10.1103/PhysRevLett.116.015002

[40] Lesur M, Itoh K, Ido T, Osakabe M, Ogawa K, Shimizu A, Sasaki M, Ida K, Inagaki S, Itoh S I and the LHD Experiment Group 2016 *Phys. Rev. Lett.* **116**(1) 015003 URL https://link.aps.org/doi/10.1103/PhysRevLett.116.015003

[41] Wang H, Todo Y, Ido T and Suzuki Y 2018 *Phys. Rev. Lett.* **120**(17) 175001 URL https://link.aps.org/doi/10.1103/PhysRevLett.120.175001

[42] Osakabe M, Ido T, Ogawa K, Shimizu A, Yokoyama M, Seki R, Suzuki C, Isobe M, Toi K, Spong D A, Nagaoka K, Takeiri Y, Igami H, Seki T, Nagasaki K and the LHD Experiment Group 2014 Indication of bulk-ion heating by energetic particle driven geodesic acoustic modes on LHD *25th IAEA Fusion Energy Conference Proceedings*

[43] Zarzoso D, Sarazin Y, Garbet X, Dumont R, Strugarek A, Abiteboul J, Cartier-Michaud T, Dif-Pradalier G, Ghendrih P, Grandgirard V, Latu G, Passeron C and Thomine O 2013 *Phys. Rev. Lett.* **110**(12) 125002 URL https://link.aps.org/doi/10.1103/PhysRevLett.110.125002

[44] Sasaki M, Itoh K, Hallatschek K, Kasuya N, Lesur M, Kosuga Y and Itoh S I 2017 *Scientific Reports* **7** ISSN 2045-2322 URL http://dx.doi.org/10.1038/s41598-017-17011-y

[45] Sasaki M, Itoh K and Itoh S I 2011 *Plasma Physics and Controlled Fusion* **53** 085017 URL http://stacks.iop.org/0741-3335/53/i=8/a=085017

[46] Zarzoso D, Biancalani A, Bottino A, Lauber P, Poli E, Girardo J B, Garbet X and Dumont R 2014 *Nuclear Fusion* **54** 103006 URL http://stacks.iop.org/0029-5515/54/i=10/a=103006

[47] Toi K 2019 Observation of bulk ion heating via energetic-ion-driven zonal flow (EGAM) in LHD plasma *The 74th annual meeting of the Physical Society of Japan*

[48] Todo Y and Sato T 1998 *Physics of Plasmas* **5** 1321–1327 ISSN 1089-7674 URL http://dx.doi.org/10.1063/1.872791

[49] Todo Y, Berk H and Breizman B 2010 *Nuclear Fusion* **50** 084016 URL http://stacks.iop.org/0029-5515/50/i=8/a=084016

[50] Todo Y, Seki R, Spong D A, Wang H, Suzuki Y, Yamamoto S, Nakajima N and Osakabe M 2017 *Physics of Plasmas* **24** 081203 ISSN 1089-7674 URL http://dx.doi.org/10.1063/1.4997529

[51] Todo Y 2017 A new magnetohydrodynamic hybrid simulation model with thermal and energetic ions *The 26th International Toki Conference (ITC-26) and The 11th Asia Plasma and Fusion Association Conference(APFA-11)*

[52] Todo Y 2016 *New Journal of Physics* **18** 115005 URL http://stacks.iop.org/1367-2630/18/i=11/a=115005

[53] Goldston R J and Rutherford P H 1995 *Introduction to plasma physics* (Institute of Physics Publishing) chap 14, pp 229–248

[54] Suzuki Y, Nakajima N, Watanabe K, Nakamura Y and Hayashi T 2006 *Nuclear Fusion* **46** L19 URL http://stacks.iop.org/0029-5515/46/i=11/a=L01

[55] Zarzoso D, del Castillo-Negrete D, Escande D, Sarazin Y, Garbet X, Grandgirard V, Passeron C, Latu G and Benkadda S 2018 *Nuclear Fusion* **58** 106030 URL http://stacks.iop.org/0029-5515/58/i=10/a=106030